ISSN 1070-3284, Russian Journal of Coordination Chemistry, 2023, Vol. 49, No. 8, pp. 465–470. © Pleiades Publishing, Ltd., 2023.
Russian Text © The Author(s), 2023, published in Koordinatsionnaya Khimiya, 2023, Vol. 49, No. 8, pp. 451–457.

# Reactions of Triangular Molybdenum and Tungsten Clusters with Tetrabromocatechol

**P. A. Petrov[a], *, E. A. Filippova[a], V. R. Giniyatullin[b], T. S. Sukhikh[a], D. G. Sheven'[a], A. L. Gushchin[a], and M. N. Sokolov[a]**

[a] *Nikolaev Institute of Inorganic Chemistry, Siberian Branch, Russian Academy of Sciences, Novosibirsk, Russia*

[b] *Novosibirsk State University, Novosibirsk, Russia*

**e-mail: panah@niic.nsc.ru*

Received October 27, 2022; revised January 27, 2023; accepted March 10, 2023

**Abstract**—The reaction of cluster complex $(^nBu_4N)_2[Mo_3Se_7Br_6]$ with tetrabromocatechol ($H_2Tbc$) in the presence of $Et_3N$ and $Ph_4PBr$ results in the formation of $(Ph_4P)_2[Mo_3Se_7(Tbc)_3]\cdot 2MeOH$ (**Ia**·2MeOH). Under the same conditions, the tungsten analogue $(^nBu_4N)_2[W_3S_7Br_6]$ is completely or partly destroyed to give the complex $(Ph_4P)(Et_3NH)[WO_2(Tbc)_2]$ (**II**). The structures of **Ia**·2MeOH and **II** were established by X-ray diffraction analysis (CCDC nos. 2213900 and 2213901, respectively). The redox properties of complex **Ia** and related $(Ph_4P)_2[Mo_3S_7(Tbc)_3]$ (**Ib**) and $(Ph_4P)_2[Mo_3S_7(Tcc)_3]$ (**Ic**) (Tcc is tetrachlorocatecholate) were also studied by cyclic voltammetry.

**Keywords:** molybdenum, tungsten, clusters, redox-active ligands, cyclic voltammetry

**DOI:** 10.1134/S1070328423600390

## INTRODUCTION

In recent decades, there has been persistent interest in complexes of both transition and main group metals with redox-active ligands capable of existing in several oxidation states. These complexes are considered as precursors of materials with interesting magnetic, electrophysical, optical, and catalytic properties [1]. For example, a group of molybdenum cluster complexes with dithiolene ligands proved to be precursors of multicomponent molecular conductors [2–5]. Dioxolene analogues of these clusters are markedly less numerous: only tetrahalocatechol derivatives are known [6, 7]. An attempt to obtain a molybdenum sulfide cluster with 3,6-di-*tert*-butylcatecholate ($(Cat^{36})^{2-}$) resulted in the complete destruction of the cluster core and isolation of the mononuclear pentavalent molybdenum complex $[Mo(Cat^{36})_3]^-$ [8]. The reaction of $Na_2Cat^{36}$ with $[Mo_2(OAc)_4]$ also resulted in the metal–metal bond cleavage and gave $[Mo(Cat^{36})_3]^-$ [9]. Meanwhile, it is known that thiomolybdenum clusters (e.g., $\{Mo_3S_7\}^{4+}$ derivatives) are much more numerous than their analogues containing W and/or heavier chalcogens; preparation of the latter often requires development of special synthetic methods [10–13]. However, there is only one example of dithiolene complex with the $\{Mo_3Se_7\}^{4+}$ core [4], and tungsten dithiolene clusters are unknown. Here we studied the reactions of $(^nBu_4N)_2[Mo_3Se_7Br_6]$ and $(^nBu_4N)_2[W_3S_7Br_6]$ with tetrabromocatechol.

## EXPERIMENTAL

The starting clusters were synthesized according to published procedures [14]. $Et_3N$ was distilled from KOH pellets. IR spectra were measured in KBr pellets on a SCIMITAR FTS 2000 instrument. Elemental analysis was carried out on a Euro EA 3000 CHNS analyzer in the analytical laboratory of the Nikolaev Institute of Inorganic Chemistry, Siberian Branch, Russian Academy of Sciences. Cyclic voltammetry (CV) studies were performed on a Computrace 797 VA instrument (Metrohm, Switzerland). All measurements were conducted in a three-electrode electrochemical cell consisting of a glass carbon working electrode, a platinum auxiliary electrode, and an Ag/AgCl/KCl reference electrode. Acetonitrile used as the solvent was saturated with argon prior to each experiment. Tetra-*n*-butylammonium hexafluorophosphate (0.1 M solution) was used as the supporting electrolyte. The concentration of the test compound was ~1 mM. The potential sweep rate was 100 mV/s. The half-wave potential ($E_{1/2}$) was defined as $(E_a + E_c)/2$, where $E_a$ and $E_c$ refer to the anodic and cathodic peak potentials, respectively. Ferrocene was used as the internal standard (the $Fc/Fc^+$ potential is 0.43 V).

**Synthesis of $(Ph_4P)_2[Mo_3Se_7(Tbc)_3]$ (Ia).** The cluster $(^nBu_4N)_2[Mo_3Se_7Br_6]$ (254 mg, 0.12 mmol) was added to a yellow solution obtained by dissolution of $H_2Tbc$ (163 mg, 0.387 mmol) and $Et_3N$ (150 μL, 109 mg, 1.08 mmol) in acetonitrile (20 mL). The resulting dark brown solution was stirred at room temperature for 24 h and then evaporated on a rotary evaporator. The residue was extracted with methanol (10 mL + 5 mL + 5 mL) using an ultrasonic bath. The extracts were combined and filtered through a glass filter (G4), and $Ph_4PBr$ (125 mg, 0.3 mmol) was added. The brown precipitate was washed with methanol, dried, and dissolved in a $CH_2Cl_2$–methanol mixture (1 : 1). Slow evaporation of the resulting solution in air afforded single crystals of $(Ph_4P)_2[Mo_3Se_7(Tbc)_3]\cdot 2MeOH$ (**Ia**·2MeOH) suitable for X-ray diffraction. The yield was 116 mg (35%).

IR (KBr; ν, $cm^{-1}$): 3054 m, 1586 w, 1483 w, 1426 s, 1344 w, 1266 s, 1234 s, 1208 w, 1108 m, 1026 w, 997 w, 929 m, 744 m, 723 m, 688 m, 524 s, 415 w. (–)-ES-MS (*m/z*): 1055.7 ($[Mo_3Se_7(Tbc)_3]^{2-}$, 100%), 2120.0 ($[HMo_3Se_7(Tbc)_3]^-$, 10%), 2449.3 ($\{(Ph_4P)[Mo_3Se_7(Tbc)_3]\}^-$, 20%).

| For $C_{68}H_{48}O_8P_2Se_7Br_{12}Mo_3$ | | |
|---|---|---|
| Anal. calcd., % | C, 28.59 | H, 1.69 |
| Found, % | C, 28.45 | H, 1.65 |

**Synthesis of $(Ph_4P)(Et_3NH)[WO_2(Tbc)_2]$ (II).** The $(^nBu_4N)_2[W_3S_7Br_6]$ cluster (207 mg, 0.119 mmol) was added to a yellow solution obtained by dissolution of $H_2Tbc$ (162 mg, 0.387 mmol) and $Et_3N$ (150 μL, 109 mg, 1.08 mmol) in acetonitrile (20 mL). The resulting dark brown solution was stirred at room temperature for 15 h and then evaporated on a rotary evaporator. The residue was extracted with methanol (10 mL + 5 mL) using an ultrasonic bath. The extracts were combined and filtered through a glass filter (G4), and $Ph_4PBr$ (125 mg, 0.3 mmol) was added. The flaky precipitate was filtered off on a paper filter (blue ribbon). Slow evaporation of the greenish-brown solution in air resulted in the formation of pale yellow single crystals of $(Ph_4P)(Et_3NH)[WO_2(Tbc)_2]$ (**II**) suitable for X-ray diffraction. The yield was 54 mg (10%).

IR (KBr; ν, $cm^{-1}$): 3066 m, 2976 m, 1586 w, 1499 w, 1484 w, 1435 s, 1398 m, 1353 w, 1260 s, 1231 s, 1210 w, 1110 m, 1033 w, 997 w, 938 m, 908 m, 848 m, 745 m, 723 m, 686 m, 546 m, 527 s, 424 w. (–)-ES-MS (*m/z*): 982.3 (10%), 1064.2 ($[HWO_2(Tbc)_2]^-$, 100%), 1404.3 ($\{(Ph_4P)[WO_2(Tbc)_2]\}^-$, 10%).

| For $C_{42}H_{36}NO_6PBr_8W$ | | | |
|---|---|---|---|
| Anal. calcd., % | C, 33.52 | H, 2.41 | N, 0.93 |
| Found, % | C, 33.30 | H, 2.45 | N, 1.10 |

**X-ray diffraction** analysis was carried out by a standard procedure on an Bruker-Nonius X8 APEX automated four-circle diffractometer (CCD array detector, λ = 0.71073 Å, graphite monochromator) at $T = 150$ K. The reflection intensities were measured by φ-scanning of narrow (0.5°) frames. The absorption corrections were applied empirically (SADABS) [15]. The structures were solved using the SHELXT software [16] and refined using the SHELXL software [17] in the anisotropic approximation for nonhydrogen atoms using the Olex2 package [18]. The hydrogen atoms were located geometrically and refined in the rigid body approximation. The crystallographic data and X-ray experiment details are summarized in Table 1.

The full set of X-ray diffraction data for **Ia**·2MeOH and **II** are deposited with the Cambridge Crystallographic Data Centre (CCDC nos. 2213900 (**Ia**·2MeOH) and 2213901 (**II**) and are available at http://www.ccdc.cam.ac.uk/conts/retrieving.html).

## RESULTS AND DISCUSSION

The reaction of the cluster complex $(^nBu_4N)_2[Mo_3Se_7Br_6]$ with tetrabromocatechol ($H_2Tbc$) in the presence of $Et_3N$ leads to complete replacement of bromide ions by chelating tetrabromocatecholates. The addition of $PPh_4Br$ and crystallization from a $CH_2Cl_2$–methanol mixture affords the single crystals of $(Ph_4P)_2[Mo_3Se_7(Tbc)_3]\cdot 2MeOH$ (**Ia**·2MeOH). The **Ia**·2MeOH phase is isostructural to the previously reported sulfide **Ib**·2MeOH [7]. The structure of the cluster anion is typical of clusters containing the $\{Mo_3Q_7\}^{4+}$ core (Q = chalcogen). The Mo atoms form ат equilateral triangle. The Se(2), Se(4), and Se(6) atoms of the diselenide ligands lie almost in one plane with the Mo atoms, while Se(3), Se(5), Se(7) deviate from this plane in the opposite direction from the $\mu_3$-capping selenide (Fig. 1). The Mo–O distances in the *trans*-position to $\mu_3$-Se are 0.04–0.10 Å longer than the distance in the *trans*-position to the diselenide ligand. The geometry of the cluster anion in **Ia** is similar to those in related $(Ph_4P)_2[Mo_3S_7(Tbc)_3]$ (**Ib**) and $(Ph_4P)_2[Mo_3S_7(Tcc)_3]$ (**Ic**) (Tcc = tetrachlorocatecholate) (Table 2), while some elongation of the Mo–Mo and Mo–Se bond lengths is caused by the greater atomic radius of Se. The structure of **Ia**, like the structure of its analogue **Ib**, contains two methanol molecules hydrogen-bonded to each other and to the O atom of one catecholate (O(2B)···O(12), 2.877(10) Å; ∠O(2B)H(2B)O(12), 149.9°; O(4B)···O(2B), 2.702(10) Å; ∠O(4B)H(4B)O(2B), 165.7°). In addition, there are weak bonds between the methanol O atom and the axial Se atoms (O(4B)···Se(7), 2.810(8) Å; O(4B)···Se(3), 2.849(8) Å; O(4B)···Se(5), 3.110(8) Å) with distances shorter than the sum of the van der Waals radii.

**Table 1.** Crystallographic data and structure refinement details for **Ia**·2MeOH and **II**

| Parameter | Value | |
|---|---|---|
| | **Ia**·2MeOH | **II** |
| Molecular formula | $C_{68}H_{48}O_8P_2Se_7Br_{12}Mo_3$ | $C_{42}H_{36}Br_8NO_6PW$ |
| $M$ | 2854.46 | 1504.82 |
| System | Monoclinic | Triclinic |
| Space group, $Z$ | $P2_1/c$, 4 | $P\bar{1}$, 2 |
| $a$, Å | 21.1519(14) | 9.5031(6) |
| $b$, Å | 25.6984(12) | 13.2658(8) |
| $c$, Å | 14.6708(9) | 18.8517(11) |
| α, deg | 90 | 85.604(2) |
| β, deg | 99.344(2) | 83.843(2) |
| γ, deg | 90 | 74.334(2) |
| $V$, Å$^3$ | 7868.8(8) | 2272.3(2) |
| $F$(000) | 5336 | 1424 |
| μ(Mo$K_\alpha$), mm$^{-1}$ | 9.895 | 9.658 |
| Crystal size, mm | 0.25 × 0.1 × 0.07 | 0.2 × 0.13 × 0.1 |
| Data collection range of 2θ, deg | 3.722–48.812 | 3.192–52.74 |
| Ranges of $h$, $k$, $l$ | $-24 \le h \le 19$,<br>$-25 \le k \le 29$,<br>$-17 \le l \le 14$ | $-11 \le h \le 11$,<br>$-16 \le k \le 12$,<br>$-23 \le l \le 23$ |
| Number of measured, unique, and observable ($I > 2\sigma(I)$) reflections | 34798, 12935, 7956 | 31946, 9281, 8206 |
| Number of refined parameters and constraints | 905, 308 | 535, 0 |
| $R_{int}$ | 0.0951 | 0.0302 |
| GOOF on $F^2$ | 0.918 | 1.079 |
| $R_1$, $wR_2$ ($I > 2\sigma(I)$) | $R_1 = 0.0532$, $wR_2 = 0.0849$ | $R_1 = 0.0204$, $wR_2 = 0.0466$ |
| $R_1$, $wR_2$ (all reflections) | $R_1 = 0.1119$, $wR_2 = 0.0968$ | $R_1 = 0.0262$, $wR_2 = 0.0478$ |
| $\Delta\rho_{max}$, $\Delta\rho_{min}$, e Å$^{-3}$ | 1.17/–1.21 | 1.00/–0.82 |

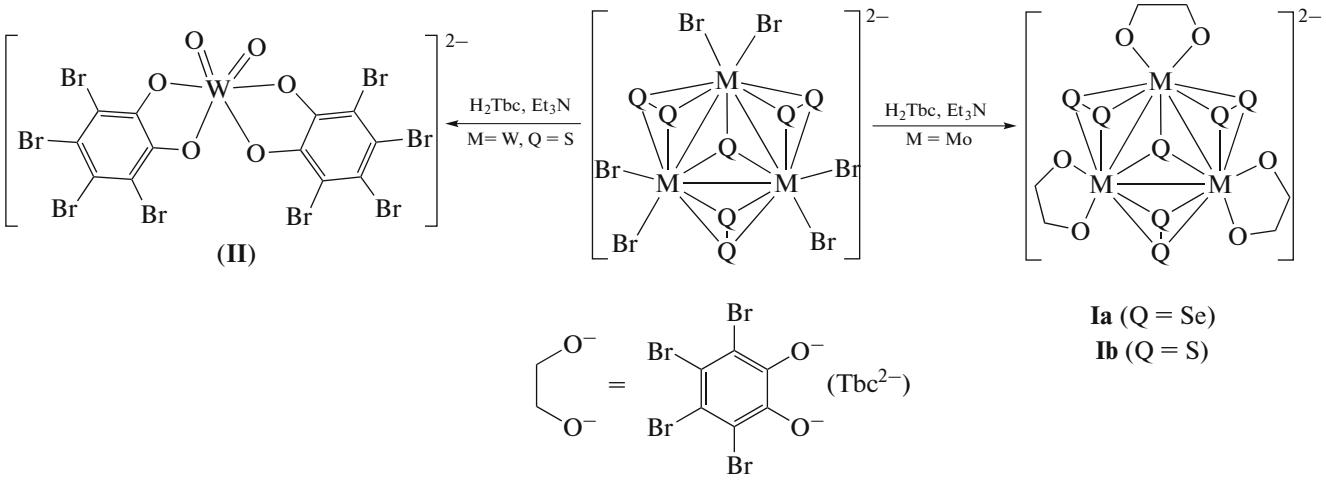


**Scheme 1.**

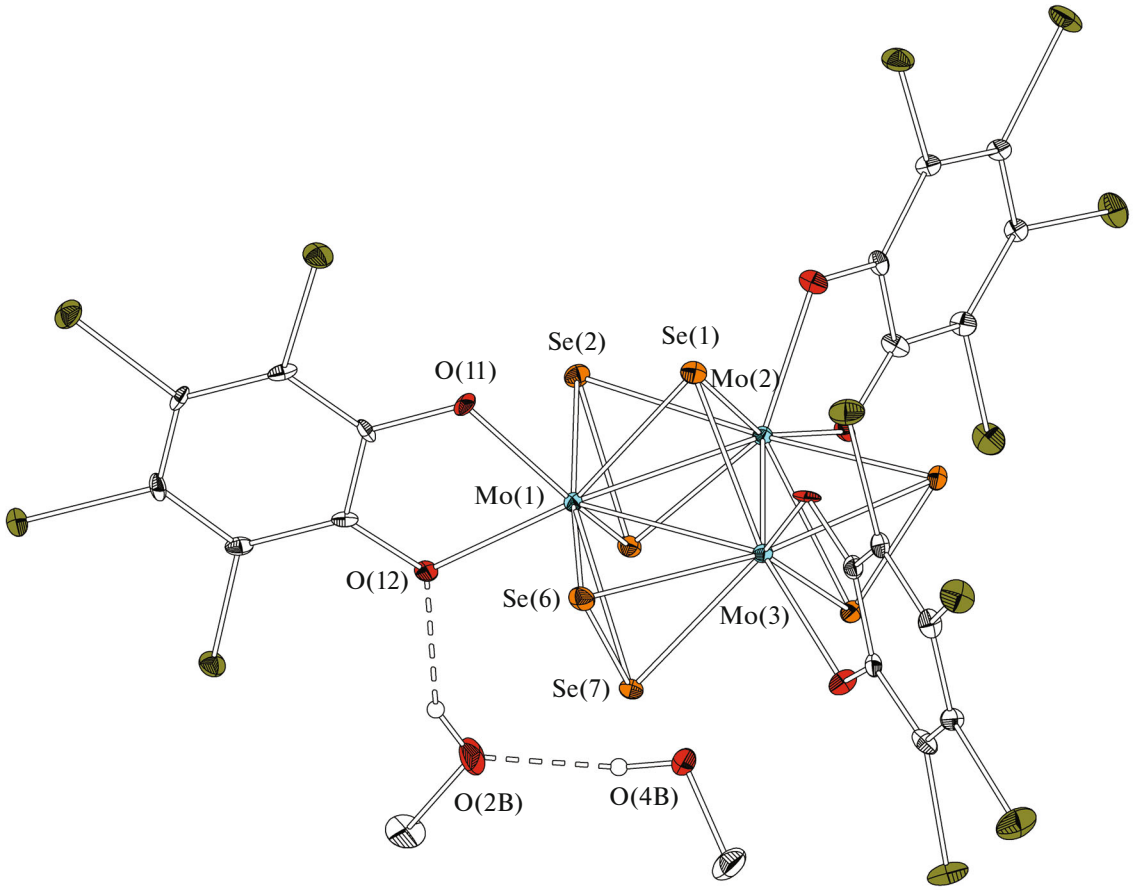


**Fig. 1.** Structure of cluster anion **Ia** (thermal ellipsoids at 30% probability).

The reaction of the tungsten cluster $(^nBu_4N)_2[W_3S_7Br_6]$ with tetrabromocatechol ($H_2Tbc$) in the presence of $Et_3N$ is accompanied by partial or complete destruction of the cluster core. After addition of $PPh_4Br$ to the reaction mixture and crystallization, it was possible to isolate only one product, mononuclear hexavalent tungsten complex $(Ph_4P)(Et_3NH)[WO_2(Tbc)_2]$ in a relatively low yield. In the complex anion, two W=O groups occur in the *cis*-conformation, which is typical of dioxo complexes of early transition metals (Fig. 2). The W=O distances are 1.7336(19) and 1.7534(18) Å, and the O(1)W(1)O(2) angle is 102.04(9)°. The $W–O_{Tbc}$ bond lengths are considerably different, and the bond in the *trans*-position to the oxo group is significantly longer (by 0.11–0.15 Å), which illustrates the strong π-donor

**Table 2.** Selected geometric parameters of the cluster anion in complex **Ia** and its analogues

| Bond | $(Ph_4P)_2[Mo_3Se_7(Tbc)_3]$ (**Ia**) | $(Ph_4P)_2[Mo_3S_7(Tbc)_3]$ (**Ib**) | $(Ph_4P)_2[Mo_3S_7(Tcc)_3]$ (**Ic**) |
|---|---|---|---|
| | *d*, Å | | |
| Mo–Mo | 2.7904(12)–2.8074(11) | 2.7501(6)–2.7647(6) | 2.7526(12)–2.7631(12) |
| Mo–($\mu_3$-Q) | 2.4768(14)–2.4885(14) | 2.3602(11)–2.3653(10) | 2.363(2)–2.369(2) |
| Mo–(μ-Q) | 2.5275(12)–2.6652(13) | 2.3972(11)–2.5348(10) | 2.398(3)–2.530(3) |
| Mo–O | 2.050(7)–2.159(6) | 2.049(2)–2.139(2) | 2.054(6)–2.115(5) |
| Angle | ω, deg | | |
| MoMoMo | 59.64(3)–60.24(3) | 59.668(17)–60.194(16) | 59.75(3)–60.13(3) |
| Ref. | This work | [7] | [6] |

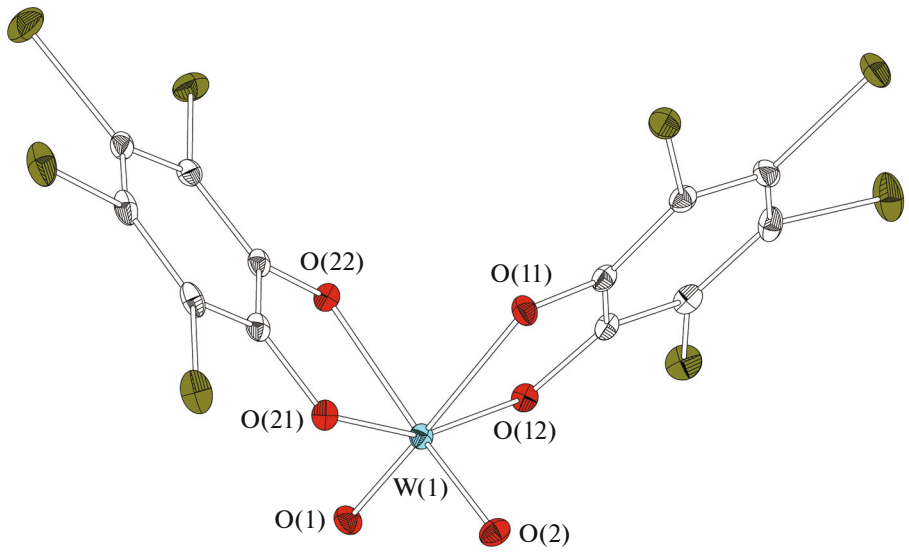


**Fig. 2.** Structure of the anionic part of complex **II** (thermal ellipsoids at 30% probability).

properties of the oxy group. As a consequence, the average W–$O_{Tbc}$ bond length (2.065 Å) in complex **II** is markedly longer than that in $[W_2(Tcc)_6]$ (1.940 Å) [19].

The composition of complexes **Ia** and **II** was confirmed by electrospray ionization mass spectrometry. The major peak for **Ia** with $m/z = 1055.7$ corresponds to the $[Mo_3Se_7Tbc)_3]^{2-}$ dianion; there is also a less intense peak with $m/z = 2449.3$ corresponding to the adduct $\{(Ph_4P)[Mo_3Se_7(Tbc)_3]\}^-$. The major peak in the spectrum of complex **II** belongs to $[HWO_2(Tbc)_2]^-$ ($m/z = 1064.2$).

The formation of complex **II**, instead of the expected $[W_3S_7(Tbc)_3]^{2-}$, may be due to the relatively easy tungsten oxidation to the highest oxidation state, in comparison with the molybdenum oxidation. It is also noteworthy that $[Mo_3S_7(Tbc)_3]^{2-}$ is stable in air both in the solid state and in solution, while $[Mo_3Se_7(Tbc)_3]^{2-}$ is formed in a lower yield and decomposes on long-term storage. Also, a ligand effect on the oxidation product can be noted: $[M_3Q_4L_3]^{2-}$ clusters (M = Mo, W; L = dithiolene) are oxidized to give pentavalent metal complexes $[M^{V}_2(\mu\text{-}Q)_2O_2L_2]^{2-}$ [20], whereas the $[W_3S_7(Tbc)_3]^{2-}$ cluster, which is presumably formed in the first stage, is apparently oxidized in air to the hexavalent tungsten complex $[W^{VI}O_2(Tbc)_2]^{2-}$ (**II**). To clarify this issue, we studied complexes **Ia**, **Ib**, and **Ic** by cyclic voltammetry (CV).

The cyclic voltammograms of complexes **Ia**, **Ib**, and **Ic** in acetonitrile (Figs. S1–S3) exhibit a group of cathodic peaks corresponding to the redox transformations of the $\{Mo_3Q_7\}^{4+}$ core and a group of anodic processes, which are determined, first of all, by the presence of the redox-active catecholate ligand. The relevant data are summarized in Table 3. The cathodic processes for all complexes are completely irreversible, since they are related to the destruction of the $\{Mo_3Q_7\}^{4+}$ core upon reduction. It is well known that the reduction of three dichalcogenide ligands in the $\{Mo_3Q_7\}^{4+}$ cluster leads to the formation of the $\{Mo_3Q_4\}^{4+}$ cluster [1]. The first anodic process is quasi-reversible (the potential difference $\Delta E$ noticeably deviates from the theoretical value of 57 mV for **Ia** and **Ib**) and is, most likely, caused by two-electron oxidation to give the neutral $[Mo_3Q_7(Tbc)_3]$ complex. The reverse cathodic peak corresponding to this process is much more intense. This noticeable shape asymmetry of the anodic and cathodic peaks may indicate deposition of electrically conducting species ($[Mo_3Q_7(Tbc)_3]$) on the electrode surface as a result of oxidation. This type of behavior was observed in earlier studies of the related $\{Mo_3Q_7\}^{4+}$ clusters with redox-active dithiolene ligands [3, 4]. In particular, in the case of $(^nBu_4N)_2[Mo_3S_7(Dmit)_3]$ (Dmit = 1,3-dithiole-2-thione-4,5-dithiolate $C_3S_5^{2-}$), a quasi-reversible two-electron oxidation was detected at 0.38 V versus Ag/AgCl. It was proven that the oxidation gave the neutral $[Mo_3S_7(Dmit)_3]$ complex, possessing electronic conductivity [3].

The presence of a heavier chalcogen (Se) in **Ia** significantly affects the position of the oxidation potential. In complex **Ia**, the first oxidation potential is observed at approximately 0.44 V (versus Ag/AgCl), while for **Ib** and **Ic**, it is shifted to anodic region by

**Table 3.** Redox potentials[a] determined for the complexes by CV in a $CH_3CN$ solution

| Compound | Oxidation, V | Reduction, V |
|---|---|---|
| $(Ph_4P)_2[Mo_3Se_7(Bbc)_3]$ (**Ia**) | 0.44[b] (119[c]), 0.80[d] | −1.49, −1.88[e] |
| $(Ph_4P)_2[Mo_3S_7(Tbc)_3]$ (**Ib**) | 0.73[b] (96[c]), 0.91[d] | −1.04, −1.89[e] |
| $(Ph_4P)_2[Mo_3S_7(Tcc)_3]$ (**Ic**) | 0.75[b] (66[c]), 0.95[d] | −1.08, −1.89[e] |

[a] $E$, V versus Ag/AgCl.
[b] Reversible, $E_{1/2} = (E_a + E_c)/2$.
[c] $\Delta E$, mV; $\Delta E = |E_a - E_c|$.
[d] Irreversible, $E_{pa}$.
[e] Irreversible, $E_{pc}$.

0.3 V. This is consistent with the general trend for the easier oxidation of selenide clusters compared to the sulfide analogues. On the other hand, a clear effect of the redox-active ligand can be followed. The oxidation potentials for **Ia**, **Ib**, and **Ic** are markedly higher than those of the dithiolene complexes $(^nBu_4N)_2[Mo_3S_7(Dmit)_3]$ (0.38 V) and $(^nBu_4N)_2[Mo_3Se_7(Dmit)_3]$ (0.15 V), i.e., the catecholate complexes are less prone to oxidation than dithiolene ligands.

## FUNDING

This study was supported by the Ministry of Science and Higher Education of the Russian Federation (project nos. 121031700313-8 and 121031700315-2).

## CONFLICT OF INTEREST

The authors of this work declare that they have no conflicts of interest.

## SUPPLEMENTARY INFORMATION

The online version contains supplementary material available at https://doi.org/10.1134/S1070328423600390.

## REFERENCES

1. Gushchin, A.L., Laricheva, Y.A., Sokolov, M.N., and Llusar, R., *Russ. Chem. Rev.*, 2018, vol. 87, p. 670. https://doi.org/10.1070/RCR4800
2. Llusar, R. and Vicent, C., *Coord. Chem. Rev.*, 2010, vol. 254, p. 1534.
3. Llusar, R., Uriel, S., Vicent, C., et al., *J. Am. Chem. Soc.*, 2004, vol. 126, p. 12071.
4. Gushchin, A.L., Llusar, R., Vicent, C., et al., *Eur. J. Inorg. Chem.*, 2013, p. 2615.
5. Gushchin, A.L., Abramov, P.A., Peresypkina, E.V., and Sokolov, M.N., *Russ. J. Coord. Chem.*, 2013, vol. 39, p. 6. https://doi.org/10.1134/S1070328413010041
6. Falvello, L.R., Llusar, R., Triguero, S., and Vicent, C., *Chem. Commun.*, 2009, p. 3440.
7. Petrov, P.A., *J. Cluster Sci.*, 2017, vol. 28, p. 1815.
8. Petrov, P.A., Afonin, M.Yu., Naumov, D.Yu., et al., *Russ. J. Coord. Chem.*, 2015, vol. 41, p. 31. https://doi.org/10.1134/S1070328415010078
9. Matsumoto, T., Yano, H., Wakizaka, M., et al., *Bull. Chem. Soc. Jpn.*, 2015, vol. 88, p. 74.
10. Petrov, P.A., Nadolinny, V.A., Bogomyakov, A.S., and Sukhikh, T.S., *New J. Chem.*, 2018, vol. 42, p. 12349.
11. Sokolov, M.N., Abramov, P.A., Gushchin, A.L., et al., *Inorg. Chem.*, 2005, vol. 44, p. 8116.
12. Gushchin, A.L., Sokolov, M.N., Peresypkina, E.V., et al., *Eur. J. Inorg. Chem.*, 2008, p. 3964.
13. Virovets, A.V., Gushchin, A.L., Abramov, P.A., et al., *J. Struct. Chem.*, 2006, vol. 47, p. 326. https://doi.org/10.1007/s10947-006-0303-y
14. Gushchin, A.L., Ooi, B.-L., Harris, P., et al., *Inorg. Chem.*, 2009, vol. 48, p. 3832.
15. *APEX2 (version 1.08), SAINT (version 7.03), SADABS (version 2.11), SHELXTL (version 6.12)*, Madison: Bruker AXS Inc., 2004.
16. Sheldrick, G.M., *Acta Crystallogr., Sect. A: Found. Adv.*, 2015, vol. 71, p. 3.
17. Sheldrick, G.M., *Acta Crystallogr., Sect. C: Struct. Chem.*, 2015, vol. 71, p. 3.
18. Dolomanov, O.V., Bourhis, L.J., Gildea, R.J., et al., *J. Appl. Crystallogr.*, 2009, vol. 42, p. 339.
19. DeLearie, L.A. and Pierpont, C.G., *Inorg. Chem.*, 1988, vol. 27, p. 3842.
20. Llusar, R., Triguero, S., Vicent, C., et al., *Inorg. Chem.*, 2005, vol. 44, p. 8937.

*Translated by Z. Svitanko*